Molecular Dynamics Simulation of Aqueous NaF and NaI Solutions near a Hydrophobic Surface

Sandeep Pal* and Florian Müller-Plathe*

International University Bremen, P.O. Box 750561, D-28725 Bremen, Germany

Received: September 28, 2004; In Final Form: February 3, 2005

We present results from molecular dynamics simulation of aqueous solutions of alkali halide salts (NaI and NaF) at the interface with hydrophobic objects. The primary objective of this study is to investigate the structural properties of the salt solutions at the hydrophobic surface. An alkane crystal has been taken as the parent model for a hydrophobic surface. A hexagonal hole was created on it, which was half a nm deep and 2.5 nm wide. The density distributions of different species (water, anions, and cations) are studied as a function of distance from the surface. While iodide prefers the interface, the fluoride ions stay inside the bulk water region. The higher concentration of iodide ions at the interface drags sodium counterions to the interface. It also decreases the water density at the interface because of steric effects of the iodide ions. The number of contacts between the surface carbons and water decreases in the case of NaI solutions but is unchanged for NaF solutions. The orientation of the water−ion and the water−water hydrogen bond vector orientations near the interface is discussed in detail.

1. Introduction

We investigate the structural and dynamic properties of water and ions near the water hydrophobic surface by molecular dynamics simulation. The electrolytes studied are NaF and NaI. The primary objective of this manuscript is to see the structural properties in terms of density and concentration of water and ions, respectively. Two different topographies of hydrophobic surfaces have been studied to see whether surface structuring influences water and ion distributions. Another important aspect is the question of whether the presence of anions at the interface changes the hydrophobic nature of the hydrophobic surface.

The related field of modeling the interface of the water/water vapor interface of an aqueous salt solution has been an active area of research. The traditional view that there are no atomic ions at the water/vapor interface has been challenged by molecular simulations.[1−9] The selective transfer of salt anions to the water vapor interface on the basis of the atomic radius and the polarizability of the ions have been investigated by molecular dynamics simulations.[5−8] The traditional interpretation of this observation in terms of the Gibbs adsorption equation[1−3] is that the alkali halide salts are repelled from the solution/air interface. Consequently, the generally accepted view has been for many decades that the interface of aqueous electrolyte solutions is devoid of ions, although there have been no direct measurements with molecular resolution to support this view. It has been shown by the work of Jungwirth et al.,[6,7] using molecular dynamics simulations of a series of sodium halide solutions, that an increase of surface tension does not necessarily imply ion depletion. In fact, it was shown that, whereas the small, nonpolarizable fluoride anion is excluded from the interface, in accord with the traditional picture, all of the larger, polarizable halide anions are present at the interface, and bromide and iodide actually exhibit surfactant activity (enhanced concentration at the interface relative to the bulk).

Jungwirth et al.[6,7] modeled the air/solution interface by performing 1 ns molecular dynamics simulations at 300 K of water slabs containing sodium halide (fluoride, chloride, bromide, or iodide) salts at 1.2 M concentration. The most important ingredient used in their simulations is a polarizable potential for both water and the ions.[8] In the NaF solution, both ions are strongly repelled from the surface, leaving an ion-free layer roughly 3.5 Å thick (i.e., approximately the diameter of one water molecule). In contrast, iodide ions occupy a significant portion of the water/vapor interface. The affinity of large anions for the interface was interpreted in terms of anisotropic solvation, which induces a substantial dipole on the ion. The resulting favorable dipole−dipole interactions compensate for the loss of ion−dipole interactions that accompany the transfer of an ion from the bulk solution to the interface. The simulations were analyzed in their article by comparing with the measurements of differences in surface potentials between ionic solutions and pure water. Experiments[10−15] show a positive surface potential, which implies the presence of an ionic double layer near the surface with its positive side directed into the bulk solution.

It has been shown by molecular dynamics (MD) simulations of aqueous ionic solutions of different concentrations for two different salts of different anion size (NaCl and NaF at 300 K[16] in explicit water) that the larger anion Cl^- leads to a smaller increase in surface tension than the smaller F^- ion. The results presented in this simulation are in good agreement with the experimental data.[3]

A second area related to the present study is the solution behavior of small hydrophobic solutes and, in particular, its variation with ion type and salt concentration. The thermodynamic and structural properties of the hydration of hydrophobic solute molecules in three tetramethylammonium [$N(CH_3)_4^+$] salt solutions at various concentrations obtained from molecular dynamics simulations have been studied in detail by Kalra et al.[17] The chemical potential of hard-spheres solutes was obtained using test-particle insertion to display both salting-in (increased solubility) and salting-out (decreased solubility) effects, depending on the type of salt. Small and strongly hydrated fluoride ions are excluded from the vicinity of the hydrophobic solutes,

10.1021/jp045601h CCC: $30.25
Published on Web 03/08/2005

leading to an increase of the local water density near the hydrophobic solute, which leads to salting-out. Opposite behavior has been observed for large, less-favorably hydrated bigger ions, which associate strongly with hydrophobic solutes.

Molecular dynamics simulations were performed by van der Vegt et al.[18,19] to study the hydration thermodynamics of methane infinitely diluted in binary cosolvent/water mixtures. The additives sodium chloride (NaCl), dimethyl sulfoxide (DMSO), and acetone were studied at various additive/water ratios and analyzed in terms of solute−solvent energy and entropy changes upon solute insertion. The salting-in and salting-out behavior of the cosolutes was analyzed in terms of the solvation free energy as well as the liquid structure in the vicinity of the methane molecule. NaCl is shown to salt out methane as the result of an unfavorable solute−solvent entropy change. Acetone and DMSO salt in nonpolar solutes. Addition of acetone to water facilitates formation of empty molecular-sized cavities causing the salting-in process to be largely entropy driven.

Molecular dynamics simulations were performed on our system containing one *n*-eicosane ($C_{20}H_{42}$) crystal in contact with aqueous sodium iodide and sodium fluoride solutions. Two surface topographies were considered: (a) planar crystal without any surface structuring and (b) hexagonal holes on both sides of the crystal. Our previous[20] simulations showed an enhancement in the hydrophobicity because of surface structuring. This result was obtained for a pure water phase. In the present contribution, we investigate if this effect is also present for salt solutions, or if the holes trap ions and a charged surface is formed.

The alkali salts chosen for our simulations are NaF and NaI. Of the common halide anions, F^- is the smallest and I^- is the largest. Hence, any effect of ion diameter should be most pronounced between these two. The steric effects should also dominate over polarizability effects so that a nonpolarizable force field is sufficient.

The main objective of this work is the distribution of water and ions near the hydrophobic surface. Differences between the hydrophobic surface and the solution/vapor interfaces are of interest as the difference between the flat and the structured surface. Finally, we investigate differences in the wetting behavior between pure water and the two salt solutions.

2. Computational Details

2.1. Details of the Surface Structure. A crystal of *n*-eicosane molecules ($C_{20}H_{42}$) (one layer of 7 × 12 molecules) serves as the model of the hydrophobic surface. *n*-Eicosane has a triclinic crystal structure.[21−23] We used an idealized model surface for the *n*-eicosane crystal with no defects, Figure 1. Instead of nonbonded interactions between alkane molecules, springs were used between carbons of any chain and carbons of its six nearest neighbors, taking into account periodic boundary conditions. More specifically, springs linked carbons of the same index (i.e., $C_i - C_i'$, length 0.497 nm) and carbons one index apart ($C_i - C_{i+1}'$, length 0.89 nm). These lengths were chosen to maintain the crystal structure of *n*-eicosane in constant pressure simulations. This rigidification was necessary not so much for the parent planar alkane slab but to prevent surface reconstruction of structured alkane surfaces, which also contained shorter alkane chains.

Figure 2 shows how a structured surface is generated from the $C_{20}H_{42}$ crystal by shortening selected chains. We have tried two topographies, a hexagonal hole (19 alkane molecules shortened by four carbons) and the parent planar crystal. The schematic of the hole is shown in Figure 3. Measuring between

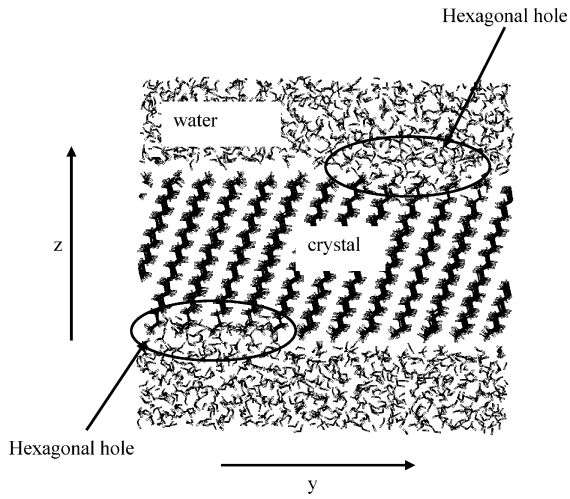

Figure 1. System chosen for our MD simulation. One hole per side of the alkane slab is indicated in the figure.

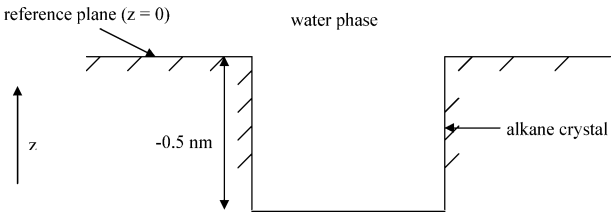

Figure 2. Schematic of the hole. The reference height ($z = 0$) is the average of the terminal methyl carbons. The depth of the hole is ∼0.5 nm.

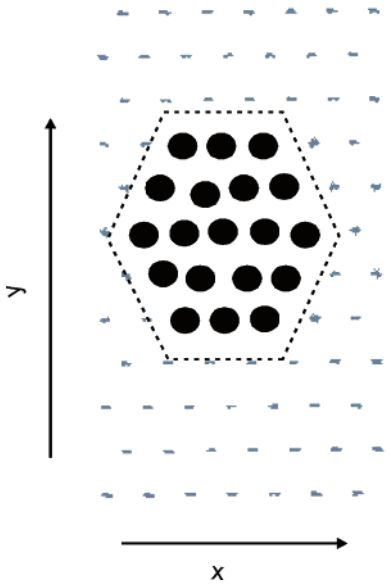

Figure 3. Schematic representation of a hexagonal hole. The dark spots indicate which alkanes have been shortened by 4 carbons.

carbon chain positions flanking the holes, the hexagonal hole has a diameter of approximately 2.5 nm. To convert to the inner widths, the diameter of a CH_3 group should be subtracted from these values. The total surface area of the hole is approximately 3.8 nm^2 (1 hexagonal hole). With the surface area of the crystal of 3.3 nm × 5.3 nm, we therefore have a percentage of indented surface of 21.8% (hexagonal hole). To increase sampling, surface indentations were used simultaneously on both the upper and lower crystal, separated from one another by 2 nm in the *y* direction and 1 nm in the *x* direction (cf. Figure 1).

2.2. Simulation Model. The periodic simulation box (3.3 × 5.3 × 5.1 nm^3) contained 1500 molecules of water, 84

TABLE 1: Ion Lennard−Jones Parameters (σ, ϵ) and Charges Used in the Simulations

ion/water	σ_{io} (nm)	ϵ_{io} (kJ/mol)	charge (e)	reference
Fluoride	0.3143	0.6998	−1	33
Iodide	0.4168	0.5216	−1	33
Sodium	0.2876	0.5216	+1	33

n-eicosane molecules, and 90 cation−anion pairs. The corresponding molar concentration of the salts in solution is 3.12 M (mol/L). For statistical accuracy, the concentration chosen was ∼3 times higher than in the article by Jungwirth et al.[6,7] For direct comparison, we have also performed a few simulations at 1.2 M concentration, and they are discussed later in the article. The sodium halide salts dissolved without precipitating at both concentrations. The crystal structure is triclinic ($\alpha = 67.6°$, $\beta = 83.9°$, $c = 2.544$ nm) and close to the experimental one ($\alpha = 68.2°$, $\beta = 85.7°$, $c = 2.743$ nm).[22,23] The difference in c comes from c being the slab thickness (simulation) and unit cell length (experiment). The eicosane crystal (thickness 2.5 nm) was separated from its periodic image by a water layer (thickness 2.6 nm). This thickness is enough for the water to reach bulk behavior between the two surfaces. The crystal plane was the *xy* plane with the inclination of the molecular axes in *y* direction. In all analyses, $z = 0$ refers to the surface of the planar crystal defined by the arithmetic mean of the *z* coordinates of all the unindented surface carbons so all indentations carry a negative *z* (Figure 3). The hexagonal hole topography on the surface of the crystal was made by switching off the interactions between the first four carbons (depth ≈ 0.5 nm) and the hydrogens connected to them and the water.

We used the YASP simulation package.[24] The system was weakly coupled to the desired temperature (298 K) with a relaxation time of 0.2 ps.[25−27] The Cartesian diagonal components of the pressure tensor were coupled separately to an external pressure of 0.1013 MPa with a relaxation time of 0.5 ps.[25−27] Bond lengths were constrained using the SHAKE algorithm.[28] The time step for the leapfrog integration scheme[25−27] was set to 0.002 ps, and trajectory frames were written to disk every 1 ps. Nonbonded interactions were evaluated at every time step with a cutoff radius of 0.9 nm using a neighbor list (update every 20 steps, neighbor list cutoff 1.0 nm). The simulations consisted of 1 ns of equilibration and 1 ns of data collection. The salt ions had been placed in the bulk water region at random positions at least 1 nm from the interface. Molecular dynamics simulation with a reduced time step of 0.5 fs was performed for 100 ps to remove possible overlaps. The resulting configuration was used as a starting configuration for the equilibration run. After 1 ns of equilibration, no drift or deviation of the densities and nonbonded energies were observed. The error bars in the densities and nonbonded energies were in the acceptable limit of ∼1%. The *n*-eicosane is described by the all-atom OPLS model.[29,30] The OPLS-AA model has been chosen because it produces realistic interactions with the SPC/E[31,32] water model. As a test, we have calculated the free energy of hydration for octane (−9.2 kJ/mol, experimental −9.87 kJ/mol). Water is treated with the SPC/E model.[32] The potential parameters of the electrolytes are shown in Table.1. They have already been shown to give good structural and dynamic properties in aqueous solutions. The article by Koneshan et al.[33] describes the modulation in the structure of the hydration shell around the alkali and the halide ions as a function of the charge and size of the corresponding ions (Table 1). Lennard−Jones parameters for interactions between unlike atoms were evaluated using the

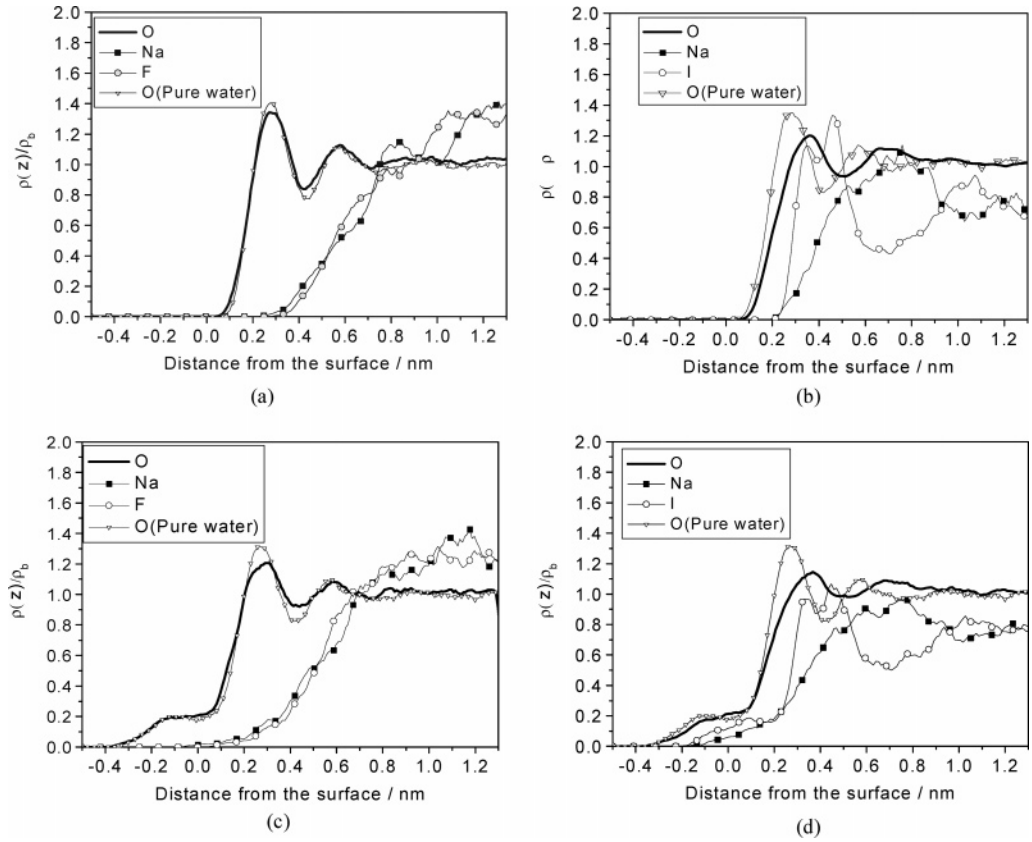

Figure 4. Number densities, $\rho(z)$, of water oxygen atoms and ions plotted vs distance from the surface in the direction normal to the interface (z), normalized by the densities of species in bulk solution at the same concentration ρ_b. (a) NaF solution near the planar surface. (b) NaI solution near the planar surface. (c) NaF solution near the surface with the hole. (d) NaI solution near the surface with the hole. For comparison, the water densities of pure water are also shown.

Lorentz−Berthelot mixing rules,[26] and electrostatic interactions were treated with the reaction field approximation[26] using an effective dielectric constant of 72.

2.3. Analysis. The simulations were analyzed in terms of the density of water and the ions at and near the interface. We have analyzed the local densities by dividing the simulation box into cells of size ($0.4 \times 0.4 \times 0.2$ nm^3) and finding the density in each cell. The absolute densities of all the species were normalized by the bulk density of the corresponding species from a separate bulk simulation of water and electrolytes at the same concentration. Since the crystal is not space fixed and has the freedom to diffuse in x and y directions, the analysis grid was attached to the crystal to get consistent density distributions over the course of the MD simulation. This was done by fixing grid points to the surface carbon atoms of the crystal. The density distribution (g/cm^3) was evaluated using

$$\rho(\vec{r}) = \frac{\left\langle N\left[\vec{r},\left(x-\frac{\Delta x}{2}, x+\frac{\Delta x}{2}\right),\left(y-\frac{\Delta y}{2}, y+\frac{\Delta y}{2}\right),\left(z-\frac{\Delta z}{2}, z+\frac{\Delta z}{2}\right)\right]\right\rangle M_s}{\Delta x \Delta y \Delta z} \quad (1)$$

where $\vec{r} = (x, y, z)$ is the center of the cell, Δx, Δy, Δz are the length of the sides of the cell, M_s is the molecular weight of the species, and $\langle N[\vec{r}]\rangle$ is the number of water oxygens inside the cell at $\vec{r}$ averaged over the 10^3 trajectory frames.

The concentrations of species have been analyzed in two different ways. First, they were analyzed by cutting the simulation box in the $x-z$ plane and finding the concentrations in the above-mentioned grid cells. The concentration (in mol/L) in a grid cell is given by

$$C_1(\vec{r}) = \frac{\rho(\vec{r})}{M_s} \times 10^3 \quad (2)$$

The ion concentrations were also analyzed in the direction normal to the interface given by the following ratio

$$C_2(z) = \frac{n_X(z)}{n_O(z)} \quad (3)$$

where $n_X(z)$ is the number of ions at a given z and $n_O(z)$ is the number of water oxygen atoms at a given z. This concentration gives the idea of the relative concentration of an ion at the interface and inside the bulk water region.

3. Results and Discussion

3.1. Density of Water and Ions near the Hydrophobic Surface. Figure 4 shows the density profiles within the liquid phase obtained by averaging over the whole simulation. The absolute density of a given species is divided by the corresponding density in bulk solution. The bulk densities of Na^+ ion in NaF and NaI bulk solutions are 0.071 g/cm^3 and 0.061 g/cm^3, respectively. The bulk densities of F^- and I^- in NaF and NaI solutions are 0.062 g/cm^3 and 0.33 g/cm^3, respectively. This way of scaling is different form the scaling done by Jungwirth et al.[6,7] as they scale the absolute densities of all species by the bulk *water* density. A difference between the sodium cation and fluoride anion on one hand, and the heavier iodide anion on the other hand, is evident in the density profiles. In the case of the NaF solution near the planar surface, Figure 4a, both ions stay away from the surface, leaving an ion-free layer roughly 0.35 nm thick (i.e., approximately the diameter of one water molecule). Because of the presence of the ion-free layer, the fluoride and sodium ions are pushed into the bulk water region and, therefore, have $\rho(z)/\rho_b > 1$ at distances ≥ 0.8 nm. In contrast, iodide ions (Figure 4b) occupy a significant portion of the interface. They also drag a certain fraction of sodium cations to the interface, showing a formation of a double layer near the interface. The ratio of the densities of ions in Figure 4b is below one in the bulk water region (0.8 nm), implying that the ions favor the interface. One of the interesting differences in the case of a NaI electrolyte between our simulations and the one performed by Jungwirth et al.[6,7] is the presence of a double peak at the water/hydrophobic surface interface rather than a single peak observed in the water/vapor interface by Jungwirth et al. This is not an effect of concentration; we have performed a simulation of a solution of 1.2 M NaI in water near the planar surface. It shows the same double-peak structure (data not shown). However, a separate simulation of NaI solutions at water/vacuum interface does not show the double peak (data not shown). The peak splitting ($\sim$0.1 nm) of the iodine is possibly due to the corrugation of the hydrophobic surface, which leads to two iodine populations near the surface.

Figure 4a and b also show the density as a function of z of pure water without salt. Here, it is evident that in the NaF solution, water wets the surface nearly like pure water (Figure 4a). In the NaI solution, there is less water at the surface than in pure water as it is being displaced by the iodide.

The density profiles of NaF and NaI electrolyte solutions near the surface with the hexagonal hole, Figure 4c and d, show that fluoride ions stay primarily in the bulk water region, whereas iodide ions enter the hole. In case of the NaF electrolytes, the sodium and fluoride ions can come nearer to the corrugated surface ($z = 0$) than to the planar crystal, because of the presence of the hole. However, their relative density at $z \approx 0$ nm is small (Figure 4c). Iodide, on the other hand, enters the hole, albeit at a small concentration ($\rho(z)/\rho_b < 0.2$), Figure 4d, and it takes some Na^+ with it for electroneutrality. The water density profile for the NaF solution is almost unchanged compared to that of pure water (Figure 4c). For the NaI solution, one notes a displacement of water above the surface ($z > 0.1$ nm) similar to the behavior at the planar surface (Figure 4b). The amount of water entering the hole is, however, also unchanged for NaI solutions. The low ion content in the hole cannot displace much water.

3.2 Preferential Interaction Coefficients Calculated from the Density Profiles. We convert the density profiles from the previous section to preferential interaction coefficients, and we estimate the infinitesimal free energy changes of the hydrophobic surface upward on addition of solute (NaF or NaI) at the concentration of 3.12 M for the NaI and NaF salts. This is not a calculation of the free energy change because of a finite concentration of salt, which would require work beyond the scope of this contribution. Still, these results show trends in the hydrophobicity of both the surfaces that support our previous findings.

The depletion or enhancement in the concentration of a salt (X) near a macromolecule in general or a hydrophobic surface (S in this contribution) can be quantified by the preferential interaction coefficient Γ.[34] They[34] relate the change of the excess chemical potentials of the macromolecule/surface to changes in the chemical potentials of water (W) and salts through the Gibbs−Duhem like relationships.[34]

$$d\mu_S = -\Gamma_{SX} d\mu_X$$
$$d\mu_S = -\Gamma_{SW} d\mu_W \quad (4)$$

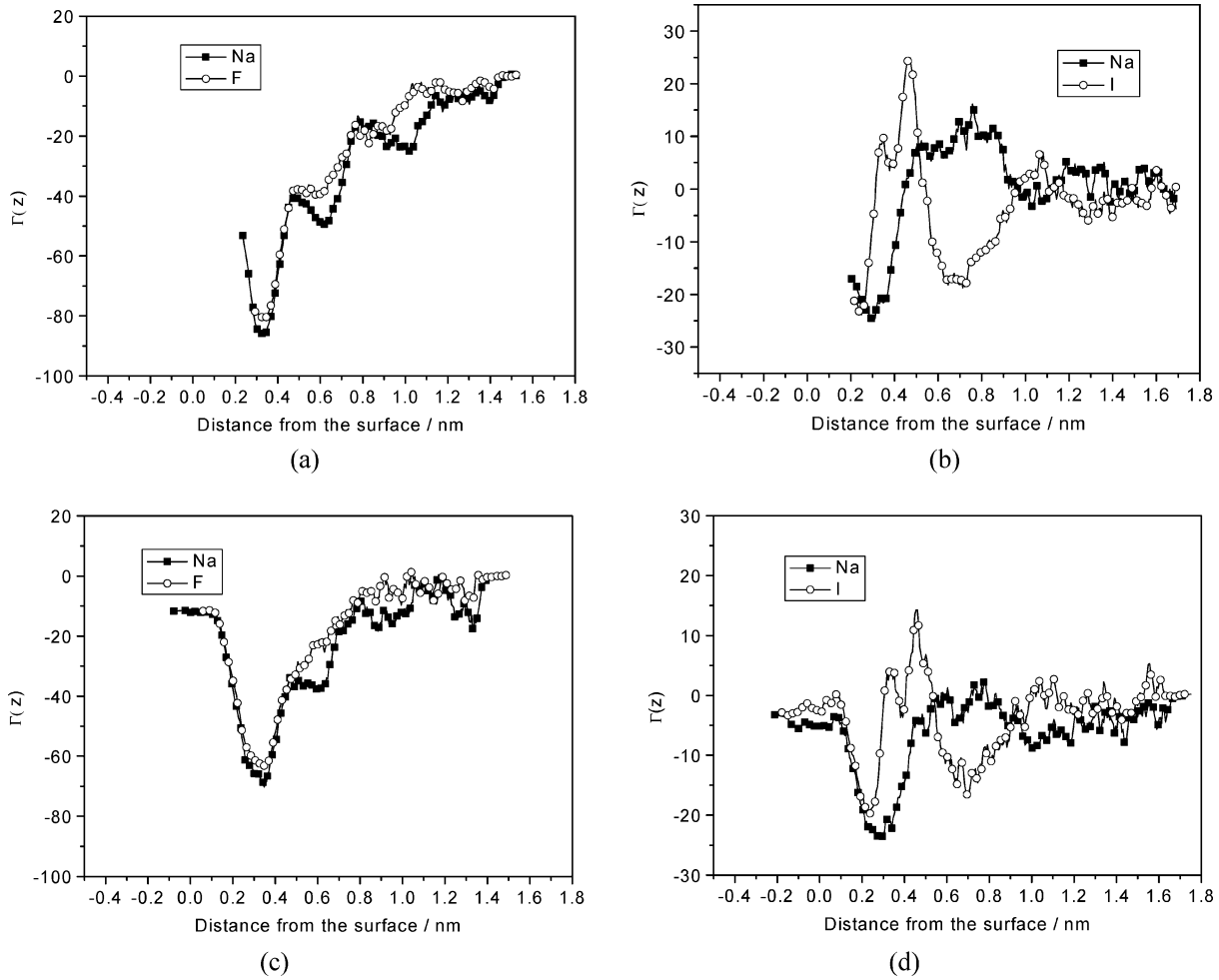

Figure 5. Γ(*z*) (defined in eq 1) as a function of *z*. (a) NaF solution near the planar surface. (b) NaI solution near the planar surface. (c) NaF solution near the surface with the hole. (d) NaI solution near the surface with the hole.

where μ refers to the chemical potential. If the preferential interaction coefficient is positive, the salt accumulates at the surface. Conversely, if the preferential interaction coefficient is negative, the ions are excluded from the surface.[34]

For an infinite planar surface in contact with a solution of water and salt, the relation between the changes in the free energy of the surface dG_S and the changes in the salt and water chemical potentials is given by[34]

$$\begin{aligned} dG_S &= -\int_0^\infty [N_X(z)d\mu_X + N_W(z)d\mu_W]dz \\ &= -\Gamma_{SX}d\mu_X \\ \Gamma_{SX} &= \int_0^\infty \left(N_X(z) - N_W(z)\frac{N_X(\infty)}{N_W(\infty)}\right)dz \\ &= \int_0^\infty \Gamma_{SX}(z)dz \end{aligned} \tag{5}$$

$N(z)$ denotes the number density of particles as a function of z from the surface (∞ denotes the bulk region away from the interface). The preferential interaction coefficient Γ_{SX} for an electrolyte is calculated as the arithmetic mean of the contributions from both ions. The variation in the $\Gamma_{SX}(z)$ as a function of distance from the surface (z) is shown in Figure 5a−d for all cases. $N(\infty)$ is calculated by averaging the number density of species (water/salt) for $z > 1.2$ nm. The integral in eq 5 was calculated between the limits $z = 0$ and $z = 1.8$ nm using the trapezoidal rule and 500 meshpoints. The preferential interaction coefficient, Γ, calculated from eq 5, are −32.6 and −2.15 for the NaF and NaI solutions in contact with a planar surface and −30.1 and −9.14 for the for NaF and NaI solutions, respectively, for the surface with the hole.

To calculate the infinitesimal change in the free energy of the surface due to the addition of salt from eq 5, we need the change in the chemical potential of the solute. The following Gibbs−Duhem equation applies

$$d\mu_X = -\frac{x_W}{x_X}d\mu_W \tag{6}$$

where x denotes the mole fraction. The change in the chemical potential of water $d\mu_W$ in the solution, upon adding a solute, is approximated by

$$\Delta\mu_W = k_B T \ln(a_W) \tag{7}$$

where a_W is the activity of water. If the mole fraction of water is high, the activity is approximately equal to the mole fraction of water x_W. In our case, the mole fraction of water, considering the ions separately is ∼0.9 (1500/1680). Therefore, the change in the chemical potential for water upon adding salt can be approximated as

$$\Delta\mu_W \approx k_B T \ln(x_W) \tag{8}$$

By substituting eq 8 in eq 2, we can calculate the changes in chemical potential of the salt. Therefore, from eq 5, and using

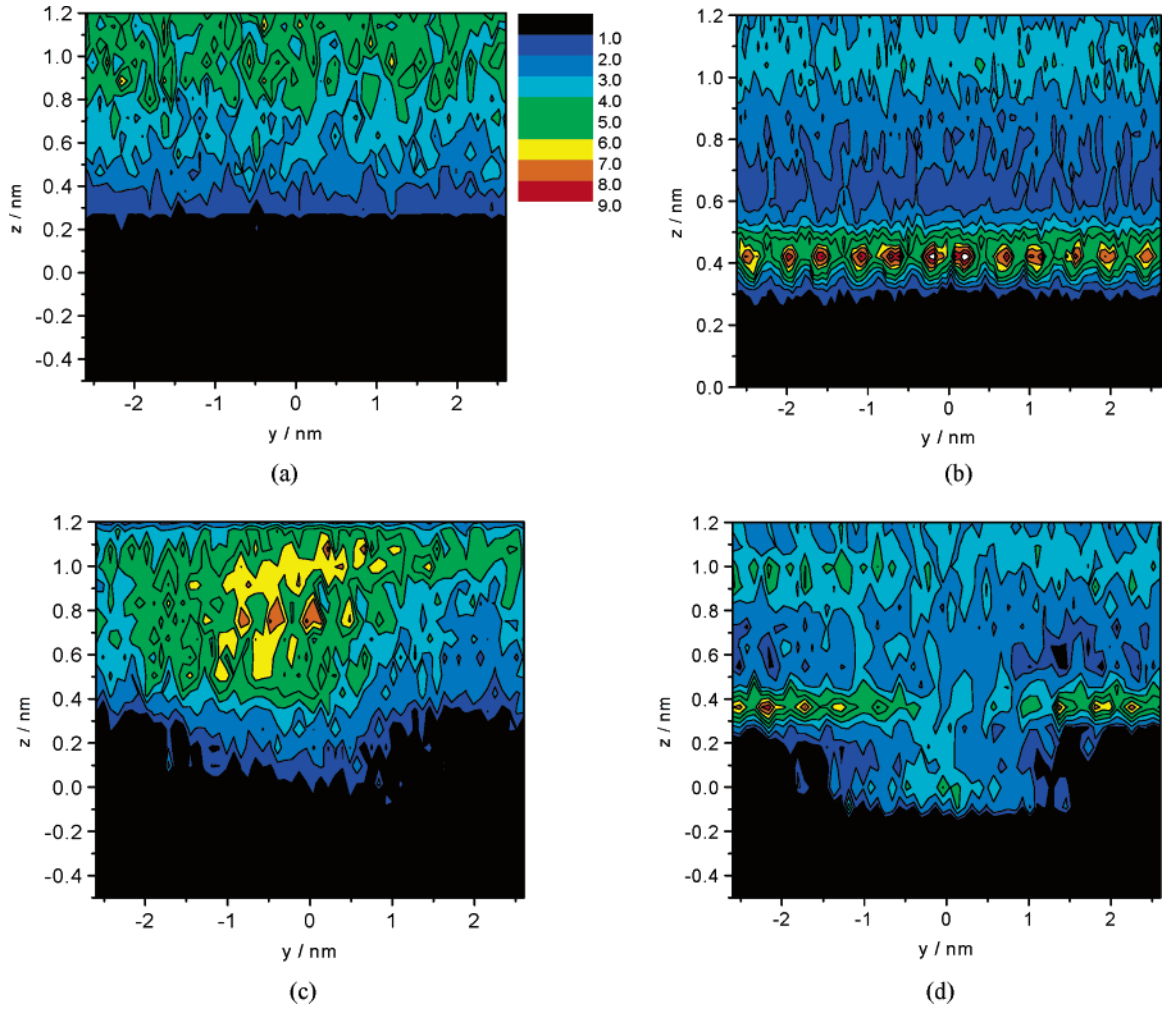

Figure 6. Concentration $C_1(\vec{r})$ in mol/l of the anions in a vertical (yz) slab of thickness $\Delta x = 0.5$ nm cutting through the center of the hole (surface with hole). (a) NaF solution near the planar surface. (b) NaI solution near the planar surface. (c) NaF solution near the surface with the hole. (d) NaI solution near the surface with the hole.

the values of the preferential interaction coefficients previously calculated, the changes in the surface free energy ΔG_s per unit area of the hydrophobic surface ($2 \times 3.3 \times 5.3$ nm^3) are 6.93 mN/m and 0.45 mN/m for NaF and the NaI solution at the planar surface and 6.40 mN/m and 1.94 mN/m for NaF and NaI solution at the surface with the hole, respectively. The changes in the surface tension of the water/water vapor interface because of addition of NaF and NaI in water at 1.2 M concentration have been calculated to be 3.6 mN/m and 1.2 mN/m, respectively.[35]

The values of all Γ_{SX} are negative, indicating a net depletion of both salts near both surfaces and leading to an increase of surface free energy (and hence hydrophobicity) upon further addition of salt. This is at first surprising, since ion densities show an accumulation of iodide ions at hydrophobic interfaces (Figure 4b and d). A look at the integrands $\Gamma_{SX}(z)$ of eq 5 for the individual ions helps in understanding the reasons (Figure 5). Figure 5a and c show that NaF is repelled from both surfaces and that Na^+ and F^- have similar density profiles. Both ions contribute to the negative integral in the same way. In contrast, the behavior of Na^+ and I^- is very different (Figure 5b and d). Iodide has a strong $\Gamma_{SI}(z)$ maximum immediately at the planar surface ($z \leq 0.5$ nm), followed by a depletion layer (0.5 nm $< z <$ 1.0 nm), Figure 5b. Their contributions to the integral amount to a net depletion $\Gamma_{SI} = -4.74$. Sodium ions have a high density where the I^- density is low (0.5 nm $< z <$ 1.0 nm). The enrichment region compensates the Na^+ depletion layer at the surface ($z <$ 0.5 nm), and the Γ_{SNa} of the Na^+ has a small positive value. Comparing to the surface with the hole (Figure 5d), we note that for both ions, the region of negative $\Gamma_{SX}(z)$ is almost unchanged. The positive peaks of $\Gamma_{SNa}(z)$ have, however, decreased in height. This leads to a reduction of $\Gamma_{SNa}(z)$ to -11.65 and $\Gamma_{SI}(z)$ to -6.64.

3.3. Density Profiles, Concentration Profiles of Water and Ions, and the Radial Distribution Function of Water near the Interface. Figure 6 shows the concentration plots, $C_1(\vec{r})$, in a yz slab of thickness, $\Delta x = 0.5$ nm positioned at $x_1 = -0.25$ nm, and $x_2 = 0.25$ nm relative to the central reference carbon atom inside the hole (The reference carbon atom is at $z = -0.5$ nm from the surface carbon atoms as shown in Figure 3). This slab cuts vertically through the surface and the hole, if present. For the planar crystal, the reference carbon is the central carbon at the surface of the slab. While Figure 6a shows that the fluoride ions stay away from the interface, leaving a low-density region near the hydrophobic surface, Figure 6b shows that the concentration of the iodide ions is higher at the interface than in the bulk. Figure 6a and b thus echos Figure 4a and b.

The situation becomes more complex when going from the planar surface to the hole geometry (Figure 6c and d). Fluoride still avoids the surface, and iodide is still attracted to it. For fluoride, however, the concentration is now highest at a distance from the surface ($z \approx 0.8$ nm) but above the hole, Figure 6c. This is mirrored in the Na^+ concentration, which has a maximum in the same region (not shown) for reasons of electroneutrality.

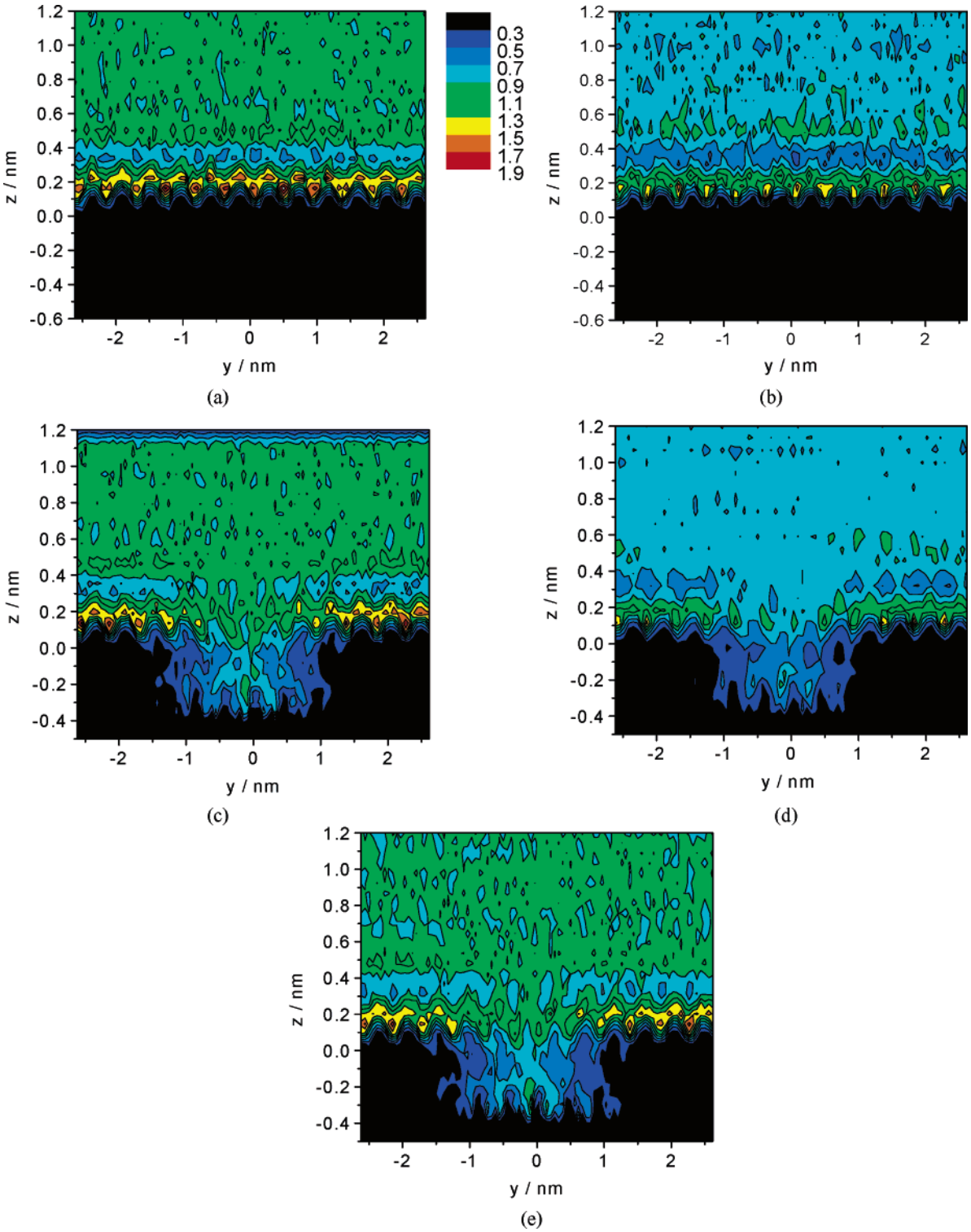

Figure 7. Water density (g/cm^3) in a vertical (yz) slab of thickness $\Delta x = 0.5$ nm cutting through the center of the hole. (a) NaF solution near planar surface. (b) NaI solution near planar surface. (c) NaF solution near surface with hole. (d) NaI solution near surface with hole. (e) Pure water near surface with hole.

The diffusion coefficients of all species, which are discussed below in section 3.3, show that there is no amorphous aggregate of ions in this region, the solution still being a liquid. The region above the hole is simply the area furthest away from any surface, so fluoride ions congregate here trying to avoid a surface.

For iodide, the hole has more obvious consequences. Iodide ions experience the bottom of the hole as just another hydrophobic surface to which they are attracted. They are found in the center of the hole, whereas, they avoid the corners and the vertical side walls. This is possible because of water structure at the edges or confinement effects. The concentration of iodide found in the hole is too low, however, for the hole to be viewed as an iodide trap.

Figure 7 shows the water density, $\rho(\vec{r})$, in the planar surface and the hexagonal hole case. For both surface geometries, the water density at the interface is higher for NaF, Figure 7a and c, than for NaI, Figure 7b and d. The presence of the bulky iodide ions at the interface leads to a lower density of water at the interface and inside the hole. Fluoride, on the other hand,

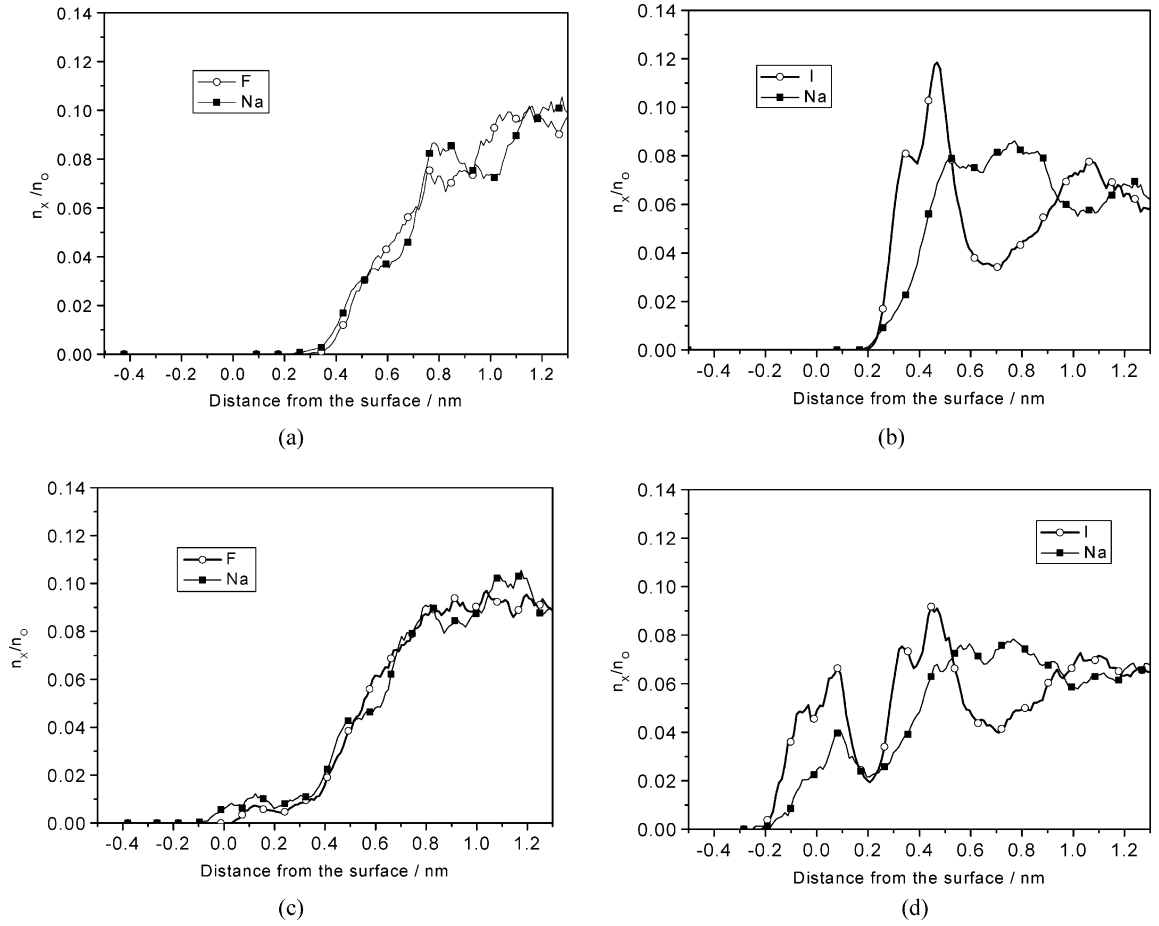

Figure 8. Ion concentration (ratio of number of ions to the number of oxygen atoms) vs the distance from the surface. (a) Fluoride and sodium concentration near the planar surface. (b) Iodide and sodium concentration near the planar surface. (c) Fluoride and sodium concentration near the surface with hole. (d) Iodide and sodium concentration near the surface with hole.

avoids the surface. The interfacial water distribution is almost identical for the NaF solution, Figure 7c, and pure water, Figure 7e.

One technical difficulty in the density and concentration plots for ions that should be mentioned is the usage of a coarser grid for the ion density (Figure 6) ($0.6 \times 0.6 \times 0.4$ nm^3) compared to that of water, Figure 7 ($0.2 \times 0.2 \times 0.1$ nm^3). The reason for using a coarser grid is purely statistical, as the number of ions is much lower than that of water molecules. Together with the interpolation scheme of the plot software, this leads to apparently larger hole sizes in the ion concentration plots (Figure 6).

In Figure 8, the ion concentrations are shown in a different normalization. They are divided by the local water concentration (i.e., $C_2(\vec{r}) = n_X(\vec{r})/n_O(\vec{r})$) to highlight changes in the relative composition. Comparing the raw concentrations (Figure 4) and the renormalized composition (Figure 8), one notes the quantitative similarity of all ion concentrations near the planar interface (subfigures a and b). Apart from a prefactor, the profiles are similar, indicating a small change of the ion/water ratio as a function of z. The situation is different in the hole geometry (subfigures c and d). For NaI, there is a significant enhancement of the ion/water ratio inside the hole (subfigure d), and even for NaF there is a small but visible increase (subfigure c). This indicates that while the concentration of ions inside the hole is reduced with respect to their bulk concentration (Figure 4c and d), the relative density of water is even more reduced.

This is also evident in the hydration number of iodide. We define the hydration number of an iodide ion as the number of oxygen atoms that are within its first hydration shell, defined by the first minimum of the iodine−oxygen radial distribution function (RDF). The RDF exhibits a maximum at 3.7−4.0 Å and a first minimum between 4 and 4.5 Å. The hydration number at a given z is found by integrating the RDF till $r = 0.43$ nm. In Figure 9, the mean iodide hydration numbers in 0.1 nm thick layers parallel to the interface are shown vs the distance z from the closest surface. The iodide hydration number near the flat interface is between 3.6 and 3.8. In the bulk, it is between 4.0 and 4.2. For the hexagonal hole case, the hydration number inside the holes is between 3.4 and 3.6. Iodide ions inside the

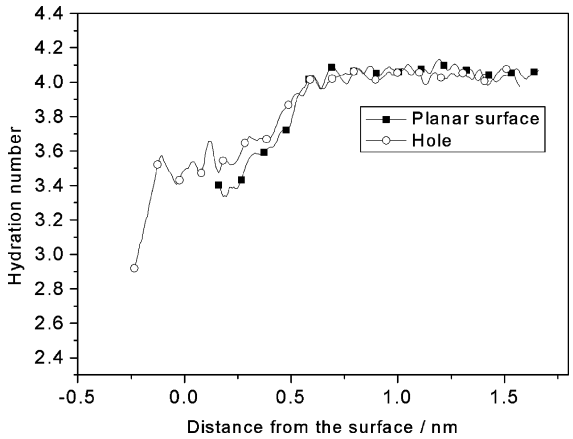

Figure 9. Average hydration number of iodide ions (water molecules in first hydration shell; for definition, see text) as a function of their distance from the surface.

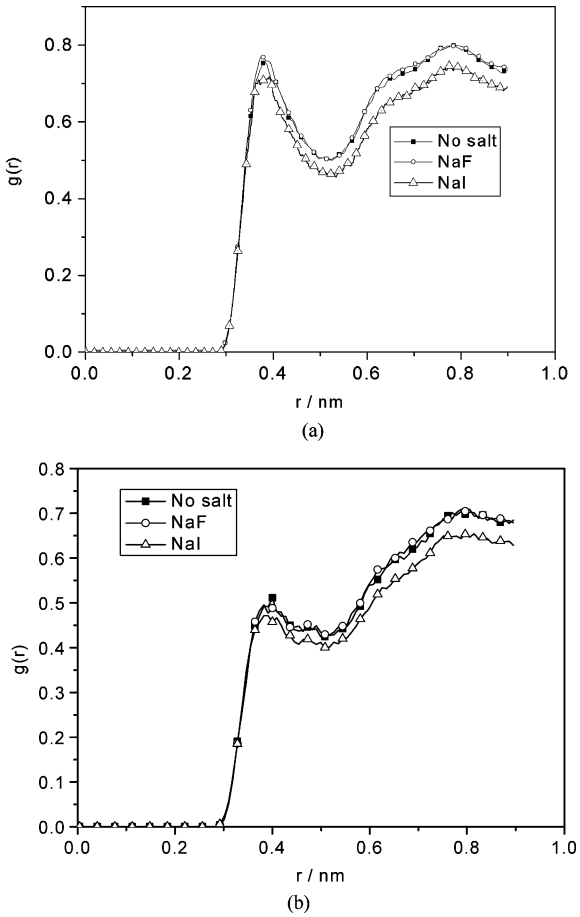

Figure 10. Radial distribution function of the surface carbons and water oxygen atoms: (a) for the planar surface and (b) for the surface with the hexagonal hole.

TABLE 2: Number of Contacts between the Water and Surface Carbons Per Water Molecule[a]

electrolyte	planar surface	hexagonal hole
NaI	0.38 (3.45)	0.25 (2.77)
NaF	0.46 (4.11)	0.29 (3.25)
pure water	0.45 (4.00)	0.28 (3.21)

[a] In parentheses, the number of contacts between the water and surface carbons per surface carbon atom is shown.

holes have on average about half a water molecule less than in the bulk. At the bottom of the hole (∼0.25 nm) the hydration number abruptly falls to below 3, so also here an iodide has approximately $^1/_2$ water molecule less than an iodide immediately at the planar surface (+0.2 nm).

Figure 10a and b shows the radial distribution function between surface carbons and water molecules. Surface carbons are the methyl carbons (C_1) at the chain ends for the planar surface. For the structured surface, the C_2-C_4 carbons lining the hole also count as surface carbons. For the NaI solution, the number of contacts between the water and the surface carbons have visibly decreased compared to those of the NaF solution and pure water for both surface topographies. In contrast, there is practically no difference between the NaF solution and pure water. By integrating the radial distribution function until the first minimum at $r = 0.5$ nm, we find the number of contacts between the surface carbons with the water molecules. The number of contacts the hydrophobic surfaces make with water is shown in Table 2. The presence of iodide reduces the water−surface contacts by approximately 10% for

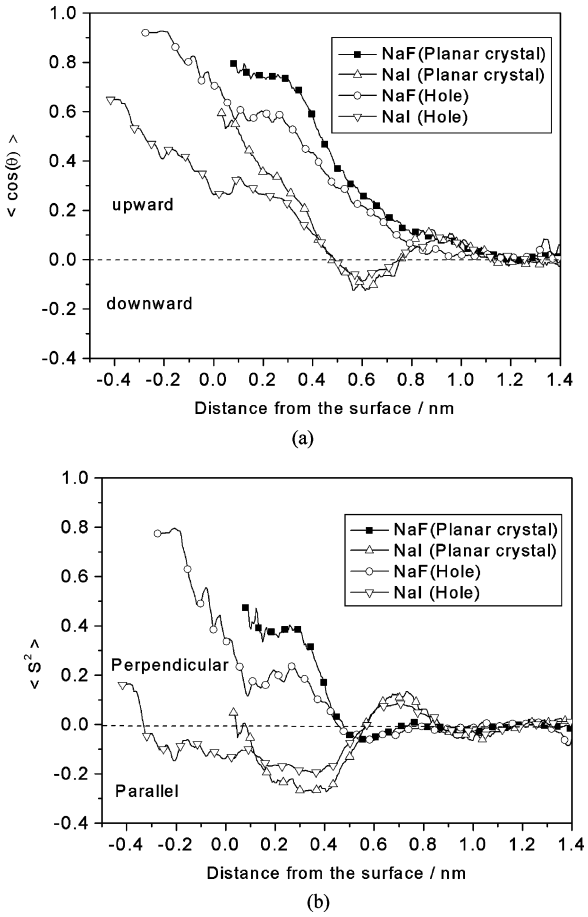

Figure 11. Orientation of the water anion hydrogen bonds. A water molecule is considered hydrogen bonded to a hydrogen-bond acceptor, A, if the O−A distance is less than a cutoff value (3.5 Å for water−water, 3.3 Å for water−fluoride, 4.3 Å for water−iodide), and the angle between O−A axis and the O−H bond is less than 30°. The orientation is reported as: (a) the cosine of the angle between the vector from the water oxygen to the acceptor atom A and the surface normal and as (b) the second Legendre polynomial $\langle S^2 \rangle$ of the cosine of the same angle.

both surface topographies; whereas, NaF slightly increases the number of water−surface contacts.

3.4. Orientation of Hydrogen Bonds. We show the orientation of water−water and ion−water hydrogen bonds in the electrolyte solutions as a function of z in Figures 11 and 12. The definition of hydrogen bonding is given in the caption of Figure 11. We define a vector pointing from the oxygen atom of the water molecule acting as the hydrogen bond donor to the atom acting as a hydrogen bond acceptor, i.e., a water oxygen or an anion. Figure 11a shows the hydrogen bond orientation of the water molecule in two different ways. First, as the cosine of the angle θ between this vector and the surface normal of the slab $\langle \cos(\theta) \rangle$. A positive value of $\langle \cos(\theta) \rangle$, means that the hydrogen bond vector points away from the surface. The orientation is, second, measured by an order parameter $\langle S^2 \rangle$ of the same angle θ, in Figure 11b.

$$\langle S^2 \rangle = 0.5 \langle 3 \cos^2 \theta - 1 \rangle \tag{9}$$

A positive value of $\langle S^2 \rangle$ implies that the hydrogen bonds prefer to align perpendicular to the surface, it is negative when the preferred alignment is parallel to the surface. It is zero at the magic angle or for random orientations.

The ion densities (cf. Figure 4) have a direct influence on the orientation of water−anion hydrogen bonds (Figure 11).

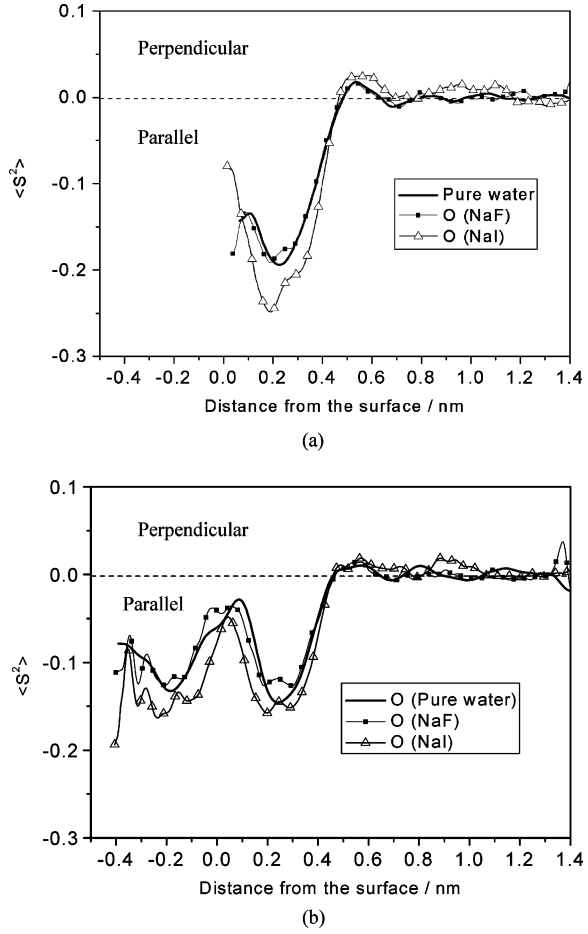

Figure 12. Orientation of water−water hydrogen bonds. (a) Near the planar surface (b) Near the surface with the hole. The definition of hydrogen bonds and orientations is the same as in Figure 10.

Close to the surface (<0.5 nm) they point away from the surface, reflecting the fact that some water molecules approach the surface more closely than the ions (Figure 11a). This is true for both anions and both surfaces. There are, however, differences between fluoride and iodide, which are best seen comparing the NaF and NaI curves for the planar interface. Fluoride avoids the surface, so water−fluoride hydrogen bonds point upward (away from the surface), and $\langle\cos(\theta)\rangle$ decays uniformly. In contrast, iodide prefers the surface, which leads to a region of negative $\langle\cos(\theta)\rangle$ between 0.45 and 0.75 nm, indicating that there is a layer of water molecules above the iodide layer, whose water−iodide hydrogen bonds point downward (toward the surface). The fact that there is at all a water layer (<0.45 nm) with hydrogen bonds pointing upward toward iodide is due to the large diameter of this anion: Although it prefers the surface, it cannot get as close as a water molecule. Beyond 0.75 nm, $\langle\cos(\theta)\rangle$ for NaI is again positive. This is explained by a secondary iodide layer at ∼1.0 nm, visible in Figures 4b and 6b. The surface topography does not influence the hydrogen−bond orientations much except that there is less order inside the hole because the vertical hole walls influence the hydrogen bond orientation, too.

The order parameters $\langle S^2\rangle$ (Figure 11b) are consistent with this picture. At close range (<0.45 nm), the water−fluoride H bonds are more perpendicular than the magic angle, whereas, the water-iodide H-bonds are more parallel because of the position of the anions (fluoride away from the surface, iodide in the surface layer).

TABLE 3: The Diffusion Coefficients (in 10^{-5} cm²/s) Parallel to the Surface $D_{||}$

system	Na^+	F^-	I^-	H_2O
		Planar Crystal		
pure water	−	−	−	16.2 ± 0.39
NaF solution	4.9 ± 1.7	5.1 ± 0.9	−	10.3 ± 0.5
NaI solution	8.2 ± 2.0	−	11.5 ± 1.5	12.8 ± 0.5
		Hexagonal Hole		
pure water	−	−	−	16.5 ± 0.31
NaF solution	3.9 ± 0.1	2.9 ± 1.0	−	7.0 ± 0.15
NaI solution	9.9 ± 2.2	−	10.0 ± 3.1	12.7 ± 0.65

[a] The average diffusion coefficients were obtained as $D_{||} = {}^1/_2(D_{xx} + D_{yy})$, their errors as $|D_{xx} - D_{yy}|$.

The water−water hydrogen bond orientation, defined by the order parameter $\langle S^2\rangle$ for both the NaF and NaI solutions, shows a preferential parallel orientation near the interface, which is a characteristic of hydrophobic surfaces, Figure 12a and b.[36] In the bulk region (>0.5 nm), the water−water hydrogen bonds show no preferred orientation. Figure 12a shows that the water−water hydrogen bonding has a parallel arrangement near (<0.5 nm), the planar surface. In the hole case, Figure 12b, there is a double minimum structure at $z = 0.3$ nm (at the interface) and $z = -0.2$ nm inside the hexagonal hole probably because of the competing influence of the hole walls. In the NaI solution, there is a stronger parallel alignment of hydrogen bonds than in the NaF solution or in pure water near both surfaces, Figure 12a and b. This orientation of the water−water hydrogen bonds is different from previous results[6,7] observed for the hydrogen bonding orientation of water. They show that in the case of NaI electrolytes near the vacuum interface, the hydrogen bond orientation is slightly disrupted and the orientation of the water−water hydrogen bond vectors point toward the bulk.

3.5. Diffusion near the Interface. Although the emphasis of this article is on the static distribution of water and ions near the interface, we have also calculated the parallel diffusion coefficient $D_{||}$ of all species in the different cases. (The perpendicular diffusion coefficient $D_\perp = D_{zz}$ cannot be evaluated because the displacement is bounded by the alkane slabs.) The Cartesian components of the diffusion coefficients were determined by calculating the center-of-mass mean-square displacements of the species and determining the slope from the linear region between 600 ps and 1 ns during the production run. The parallel diffusion coefficient was calculated from the components as

$$D_{||} = 0.5(D_{xx} + D_{yy}) \tag{10}$$

The diffusion coefficients are of the order of 10^{-5} cm²/s, showing that all systems are liquid, Table 3. The anions move faster than the cation, and I^- is faster than F^-, all in line with the experimental and simulation data.[37] The surface topography has a minor influence, if any; corresponding diffusion coefficients for the planar and the hole geometries agree to within their error limits. This means that although I^- is attracted to the surface, this attraction does not inhibit sideways translation, so the residence times at surface sites must be short.

4. Conclusions

This contribution has studied the behavior of aqueous salt solutions near a flat and a nanostructured hydrophobic surface. In many ways, the distribution of the ions follows the pattern found near the vacuum interface; small anions (F^-) avoid the surface, whereas large anions (I^-) prefer the surface. The cations (Na^+) adapt to the anion distribution. For NaF solutions, the

cation follows the anion into the bulk, for NaI solutions, the Na^+ forms a layer above the interfacial layer of I^-. The distribution of water is dictated by the salt distribution. As fluoride avoids the interface, the hydrophobic surface is in contact with a thin layer of almost pure water, and thus, the water density profile near the surface is very much that of pure water. Iodide, in contrast, is surface active and displaces water molecules from the first layer.

The density profiles were used to calculate the preferential interaction coefficients. The surface free energy increment of the planar surface and the indented surface per unit area were found to be positive because of the presence of the salts (NaF and NaI). The salts ions are preferentially excluded from the hydrophobic surface, increasing the surface free energy of the hydrophobic interface. The water molecules are oriented to form hydrogen bonds with the ions, and this effect dominates over the orientational ordering because of the surface.

The introduction of a nm-size indentation into the hydrophobic surface has different consequences for the two solutions. As fluoride, like Na^+, wants to be hydrated, it avoids the hole. Inside the hole, there is even less fluoride than above the flat surface. The low water density creates a bad hydration environment for fluoride. For iodide, the situation is different. Iodide accumulates at the hole bottom qualitatively in the same way as it accumulate against the flat surface. Still, there is no enrichment of iodide inside the holes. The low water density and the spatial constraint preclude this. Therefore, the holes cannot be viewed as traps for large anions. The finding is corroborated by the ion diffusion coefficients, which are virtually unchanged between the planar and the nanostructured surface.

The fact that surface indentations do not act as ion entrapments has important technological implications; if they did cause an increased binding of ions to the interface, they would effectively bestow negative charge on the surface, and a negative surface would lose some of its hydrophobic character. Such worries can be dispelled by the present results.

Acknowledgment. This work has been supported by collaboration with BASF AG in the framework of the BMBF Centre of Excellence for Materials simulation. We are grateful for numerous fruitful discussions with Horst Weiss, Harald Keller, Giuseppe Milano, Sylvain Goudeau, and Volker Weiss. We would also like to thank one referee for his insightful comments. We also thank the Fonds der Chemischen Industrie and John von Neumann Institute for Computing.

References and Notes

(1) Adam, N. K. *The Physics and Chemistry of Surfaces*; Oxford University Press: London, 1941.

(2) Bikerman, J. J. *Surface Chemistry: Theory and Applications*; Academic Press: New York, 1958.

(3) Chattoraj, D. K.; Birdi, K. S. *Adsorption and the Gibbs Surface Excess*; Plenum: New York, 1984.

(4) Knipping, E.; Lakin, M. J.; Foster, K. L.; Jungwirth, P.; Tobias, D. J.; Gerber, R. B.; Dabdub, D.; Finlayson-Pitts, B. J. *Science* **2000**, *288*, 301.

(5) Randles, J. E. B. *Phys. Chem. Liq*. **1977**, *7*, 107.

(6) Jungwirth, P.; Tobias, D. J. *J. Phys. Chem. B* **2001**, *105*, 10468.

(7) Jungwirth, P.; Tobias, D. J. *J. Phys. Chem. B* **2002**, *106*, 6361.

(8) Tobias, D. J.; Jungwirth, P.; Parrinello, M. *J. Phys. Chem*. **2001**, *114*, 7036.

(9) Garrett, B. C. *Science* **2004**, *303*, 1146.

(10) Dang, L. X.; Chang, T. M. *J. Phys. Chem. B* **2002**, *106*, 235.

(11) Ayotte, P.; Nielsen, S. B.; Weddle, G. H.; Johnson, M. A.; Xantheas, S. S. *J. Phys. Chem. A* **1999**, *103*, 10665.

(12) Seinfeld, J. H. *Science* **2002**, *288*, 285.

(13) Caldwell, J.; Dang, L. X.; Kollman, P. A. *J. Am. Chem. Soc*. **1990**, *112*, 9144.

(14) Perera, L.; Berkowitz, M. L. *J. Chem. Phys*. **1991**, *95*, 1954.

(15) Hu, J. H.; Shi, Q.; Dandroits, P.; Worsnop, D. R.; Zahniser, M. S.; Kolb, C. E. *J. Phys. Chem*. **1995**, *99*, 8768.

(16) Bhatt, D.; Newmann, J.; Radke, C. J. *J. Chem. Phys. B.* **2004**, *108*, 9077.

(17) Kalra, A.; Tugcu, N.; Cramer, S. M.; Garde, S. *J. Phys. Chem. B.* **2001**, *105*, 6380.

(18) van der Vegt, N. F. A.; van Gunsteren, W. F. *J. Phys. Chem. B* **2004**, *108*, 1056.

(19) van der Vegt, N. F. A.; Trzesniak, D.; Kasumaj, B.; van Gunsteren, W. F. *ChemPhysChem* **2004**, *5*, 144.

(20) Pal, S.; Müller-Plathe, F.; Weiss, H.; Keller, H. Submitted to *Langmuir*.

(21) Nyburg, S. C.; Potworowski, J. K. *Acta Crystallogr., Sect. B* **1973**, *29*, 347.

(22) Waheed, N.; Lavine, M. S.; Rutledge, G. C. *J. Chem. Phys*. **2001**, *116*, 2301.

(23) Small, D. M. *The Physical Chemistry of Lipids: From Alkanes to Phospholipids*; Plenum: New York, 1986; p 183.

(24) Müller-Plathe, F. *Comput. Phys. Commun*. **1993**, *78*, 77.

(25) Allen, M. P.; Tildesly, D. J. *Computer Simulation of Liquids*; Clarendon Press: Oxford, 1987.

(26) Frenkel, D.; Smit, B. *Understanding Molecular Simulation*; Academic Press: San Diego, 2002.

(27) Jensen, F. *Introduction to Computational Chemistry*; Wiley VCH: Chichester, 1998.

(28) Ryckaert, J. P.; Ciccotti, G.; Berendsen, H. J. C. *J. Comput. Phys*. **1977,** *23***,** 327.

(29) Duffy, E. M.; Jorgensen; W. L. *J. Am. Chem. Soc*. **2000**, *122*, 2878.

(30) Kaminski, G.; Duffy, E. M.; Matsui, T.; Jorgensen, W. L. *J. Phys. Chem*. **1994**, *98*, 13077.

(31) Berendsen, H. J. C.; Postma, J. P. M.; van Gunsteren, W. F.; DiNola, A.; Haak, J. R. *J. Chem. Phys*. **1984**, *81*, 3684.

(32) Berendsen, H. J. C.; Grigera, J. R.; Straatsma, T. P. *J. Phys. Chem*. **1987**, *91*, 6269.

(33) Koneshan, S.; Rasaiah, J. C.; Lynden-Bell, R. M.; Lee, S. H. *J. Phys. Chem. B* **1998**, *102*, 4193.

(34) Parsegian, V. A.; Rand, R. P.; Rau, D. C. *Proc. Natl. Acad. Sci. U.S.A.* **2000**, *97*, 3987.

(35) Washburn, E. W. *International Critical Tables of Numerical Data, Physics, Chemistry, and Technology*; McGraw-Hill: New York, 1928; Vol. 4.

(36) Grigera, J. R.; Kalko, S. G.; Fischbarg, J. *Langmuir* **1996**, *12*, 154.

(37) *Handbook of Chemistry and Physics*, 62nd ed.; Weast, R. C. Ed.; CRC: Boca Raton, 1993.